

Associated Spectral and Temporal State Transition of the bright ULX NGC 1313 X-1

G. C. Dewangan^{1*}, R. Misra^{1†}, A. R. Rao^{2‡} and R. E. Griffiths^{3§}

¹*IUCAA, Post Bag 4, Ganeshkhind, Pune 411 007, India*

²*Department of Astronomy & Astrophysics, Tata Institute of Fundamental Research, Homi Bhabha Road, Mumbai, 400005 India*

³*Department of Physics, Carnegie Mellon University, 5000 Forbes Avenue, Pittsburgh, PA 15213 USA*

Submitted 2009 May

ABSTRACT

Stellar mass black hole X-ray binaries exhibit X-ray spectral states which also have distinct and characteristic temporal properties. These states are believed to correspond to different accretion disk geometries. We present analysis of two long *XMM-Newton* observations of the Ultra-Luminous X-ray source (ULX) NGC 1313 X-1, which reveal that the system was in two different spectral states. While spectral variations have been observed in this source before, this data provides clear evidence that the spectral states also have distinct temporal properties. With a count rate of ~ 1.5 counts/s and a fractional variability amplitude of $\sim 15\%$, the ULX was in a high flux and strongly variable state in March 2006. In October 2006, the count rate of the ULX had reduced by a factor of ~ 2 and the spectral shape was distinctly different with the presence of a soft component. No strong variability was detected during this low flux state with an upper limit on the amplitude $< 3\%$. Moreover, the spectral properties of the two states implies that the accretion disk geometry was different for them. The low flux state is consistent with a model where a standard accretion disk is truncated at a radius of ~ 17 Schwarzschild radius around a $\sim 200M_{\odot}$ black hole. The inner hot region Comptonizes photons from the outer disk to give the primary spectral component. The spectrum of the high flux state is not compatible with such a geometry. Instead, it is consistent with a model where a hot corona covers a cold accretion disk and Comptonizes the disk photons. The variability as a function of energy is also shown to be consistent with the corona model. Despite these broad analogies with Galactic black hole systems, the spectral nature of the ULX is distinct in having a colder Comptonizing temperature (~ 2 keV) and higher optical depth (~ 15) than what is observed for the Galactic ones.

Key words: Accretion, Accretion Disks, Black Hole Physics, X-Rays: Binaries, X-Rays: Galaxies, X-rays: individual: NGC 1313 X-1

1 INTRODUCTION

Ultra-luminous X-ray sources (ULXs) are off-nuclear, compact X-ray sources with luminosities exceeding $\sim 10^{39}$ erg s⁻¹. The nature of ULXs continues to be an enigma, since their isotropic high energy output surpasses the Eddington limit of even the most massive stellar mass black holes, sometimes by large factors. One individual ULX may outshine the rest of the galaxy in the high energy X-ray band. Several models have been proposed to explain the high luminosities of ULXs. They may be powered by “in-

termediate mass black hole (IMBH)” with masses $M_{BH} \simeq 10^2 - 10^4 M_{\odot}$ (e.g., Colbert & Miller 2005) which bridge the gap between stellar mass black holes in X-ray binaries (XRBs) and super-massive black holes in active galactic nuclei. On the other hand, they may be XRBs with anisotropic emission (King et al. 2001) or beamed XRBs with relativistic jets directly pointing towards us, i.e., scaled down versions of blazars (Mirabel & Rodríguez 1999). Alternatively, they may be stellar mass black holes with super-Eddington accretion rates (Begelman 2002; King 2008).

In the absence of a direct measurement of the black hole mass in ULX, indirect evidence is provided by the spectral and temporal properties of these sources. Qualitative and quantitative similarities (and differences) between them and Galactic X-ray binaries harboring stellar mass black holes

* gulabd@iucaa.ernet.in

† rmisra@iucaa.ernet.in

‡ arrao@tifr.res.in

§ griffith@seren.phys.cmu.edu

can provide insight into their nature. The discovery of orbital modulations from the bright ULX M 82 X-1 (Kaaret et al. 2006; Kaaret & Feng 2007) and possibly from a ULX in IC 342 (Sugiho et al. 2001) implies that they too are binary systems.

Galactic X-ray binaries exhibit spectral states (e.g. see Zdziarski & Gierliński 2004, for a review). Detailed spectral modeling of these systems reveal that the accretion disks have different geometries for different states. In the high soft state, the spectra are dominated by emission from a cold accretion disk which extends probably to the inner most stable orbit. A corona or active region above the cold disk comptonizes disk photons to produce hard X-rays. In the low hard state, the disk is truncated at a larger radius and the X-rays originate from an hot inner disk. In the very high state, the geometry is probably similar to that of the high state, but here the flux from the corona is nearly equal to that of the disk. X-ray binaries are variable on a wide range of time-scales and exhibit broad band noise as well as narrow features called Quasi-periodic oscillations (QPO). Spectral state transitions are always associated with distinct changes in the rapid temporal behavior of the systems.

Both *Chandra* and *XMM-Newton* observations of ULXs have sometimes shown soft X-ray excess emission which has been interpreted as the optically thick emission from thin accretion disks with temperatures in the range of $\sim 100 - 300$ eV, which indicates that they are IMBH accreting at sub-Eddington ($\sim 0.1L_{Edd}$) rates (e.g., Miller et al. 2003; Kaaret et al. 2003; Miller et al. 2004). While this suggests that ULX may be scaled up versions of X-ray binaries, it should be noted that there are important spectral differences. Unlike X-ray binaries, a high energy spectral curvature has been detected in the the high quality X-ray spectra of a number of bright ULXs (Agrawal & Misra 2006; Stobbart et al. 2006; Goad et al. 2006; Dewangan et al. 2006; Roberts 2007). This spectral curvature is consistent with strong, nearly saturated Comptonization. Such strong Comptonization models have been invoked to explain the very high state of black hole binaries such as XTE 1550-564 (Done & Kubota 2006). However, the temperature derived for the electron plasma (~ 2 keV) is significantly smaller than that of X-ray binaries (> 20 keV).

Another striking similarity between ULX and X-ray binaries is the presence of significant variability power as well as features in the power density spectra such as QPOs and breaks (Strohmayer & Mushotzky 2003; Dewangan et al. 2006,?; Mucciarelli et al. 2006; Strohmayer et al. 2007). The QPO and break frequencies are found to be smaller than those of X-ray binaries which is taken as evidence that ULX harbor IMBH. For some sources, like the bright ULX Holmberg II X-1, the variability is absent or very weak ($< 2\%$) (Goad et al. 2006).

Studies of a collection bright ULX in nearby galaxies reveal that for some ULX a power-law spectral fit (similar to the low/hard state of X-ray binaries) is adequate while others require a thermal component (similar to the high/soft state). The temperature of the thermal component is either ~ 0.2 or ~ 2 keV suggestive of a further subdivision (Winter et al. 2006; Devi et al. 2007). These studies do not indicate whether these spectral differences represent different spectral states or if ULX themselves are a heterogeneous class comprising different kinds of sources. Long term spec-

tral variability, which is interpreted as state transitions similar to X-ray binaries, has been reported for several ULX. Repeated *Chandra* observations of the Antennae have shown hardness ratio changes in several ULXs. Transition from a high soft state to a low hard state has been observed from two ULXs in IC 342 (Kubota et al. 2001) and Holmberg IX X-1 (La Parola et al. 2001). High/hard to low/soft spectral variability has also been observed from Holmberg II X-1 (Dewangan et al. 2004).

However, these spectral variations have not been shown to be associated with temporal behavior changes and hence their identification as spectral state transitions similar to those observed in X-ray binaries remains uncertain. Moreover, the spectral variations recorded do not necessarily imply a change in the accretion disk geometry. Well constrained spectral parameters are needed for such an inference. Hence, good high quality data from two long observations of a source undergoing such changes are needed to ascertain whether ULX undergo true state transitions.

NGC 1313 is a spiral galaxy and is located at a distance of 4.13 ± 0.11 Mpc (Méndez et al. 2002). The galaxy hosts three bright and well separated X-ray sources: two ULXs X-1 and X-2, and a supernova remnant SN 1978K. NGC 1313 X-1 is one of the first ULX observed by *XMM-Newton* to show soft X-ray excess emission that led to the $\sim 1000M_{\odot}$ IMBH interpretation (Miller et al. 2003). The ULX belongs to the low-temperature, high-luminosity class in the luminosity versus temperature ($L - kT$) diagram of bright ULXs in nearby galaxies (Feng & Kaaret 2005). Feng & Kaaret (2006, 2007) have utilized the first 14 *XMM-Newton* observations and reported long term spectral variations of the two ULXs NGC 1313 X-1 and X-2. For X-1, they fitted the spectra with an absorbed power-law model and reported a correlation between the photon index, Γ and luminosity. An additional soft black body component was required for six of the observations. The short exposures of these observations (in the range of 9–41 ks), did not allow for detailed spectral and temporal studies.

Here we present detailed temporal and spectral properties of the ULX using two *XMM-Newton* observations of 123 and 20 ks. We describe the *XMM-Newton* observations and the spectral and temporal analysis in §2. In §3, the accretion disk geometries inferred from the analysis are described. We summarize and discuss the results in §4.

2 OBSERVATIONS AND DATA REDUCTION

We observed NGC 1313 with *XMM-Newton* for a 123 ks long exposure on 15 October 2006. NGC 1313 was also observed on 6 March 2006 with an exposure of 21.8 ks. We used SAS 8.0.1 with updated calibration to process and filter both EPIC-pn and MOS data. The long observation of 15 October 2006 was partly affected with low amplitude flaring particle background towards the end of the exposure. Cleaning of the flaring particle background resulted in 89.3 ks data. The observation of 6 March 2006 was not affected by particle background. For temporal analysis we selected events with patterns 0 – 12 and used either continuous exposure free of particle background or corrected for the background contribution. For spectral analysis, we selected the events with pattern 0 – 4 (single and double) for the EPIC-pn and

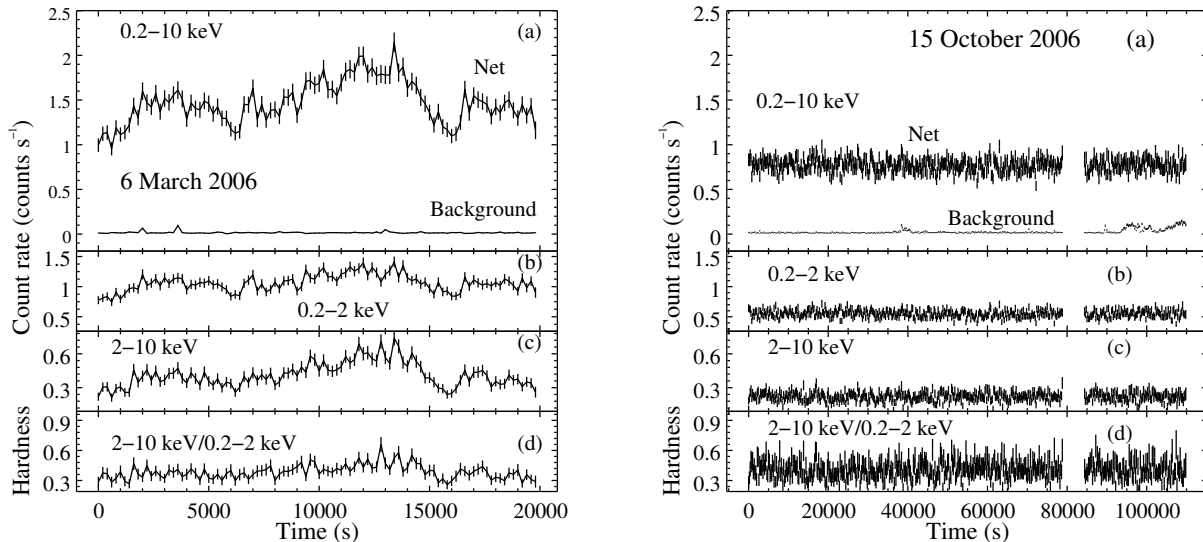


Figure 1. The background corrected EPIC-pn lightcurves of NGC 1313 X-1 binned with 200 s in the (a) 0.2 – 10 keV, (b) 0.2 – 2 keV, (c) 2 – 10 keV, and (d) the hardness ratio derived from the observations of 6 March 2006 (*left panel*) and 15 October 2006 (*right panel*). The relative contribution of background emission in the source extraction region is also shown for the 0.2 – 10 keV band.

0 – 12 for the MOS and excluded events adjacent to the bad pixels with FLAG=0. For the observation of March 2006, the source extension overlaps with the EPIC-pn chip gap and a large fraction of events have uncertain pattern. These events with poor spectral calibration were excluded from the spectral analysis but were included in the temporal analysis.

2.1 Temporal Analysis

We extracted two sets of lightcurves from each of the observations with bin sizes of 200 s and 0.5 s. A circular region of $40''$ centered at the source position was used to extract the EPIC-pn source lightcurves. We also extracted background lightcurves using four circular regions of radii $40''$ in the source-free areas and close to the source and used them to correct the source lightcurves for background contribution. In Figure 1, we show the background corrected lightcurves of NGC 1313 X-1 in the 0.2 – 10 keV, 0.2 – 2 keV and 2 – 10 keV bands. For comparison, we have also plotted the background contribution in the source extraction region. Evidently background contribution is nearly constant and negligible throughout the observations.

As can be seen in Fig. 1 (*left panel*), NGC 1313 X-1 showed strong X-ray variability throughout the observation of 6 March 2006. The most remarkable variability in the 0.2 – 10 keV band occurred at an elapsed time of ~ 13000 s when the net count rate decreased by a factor of about two in 3000 s. The hardness ratio, calculated as the ratio of count rates in the 0.2 – 2 keV and 2 – 10 keV band is also variable and correlated with the lightcurve. Thus, at high flux, the ULX has a harder spectrum.

In contrast to the 20 ks observation on 6 March 2006, the long observation of 15 October revealed that (i) the ULX was in a low flux state, X-ray emission dropped by a factor

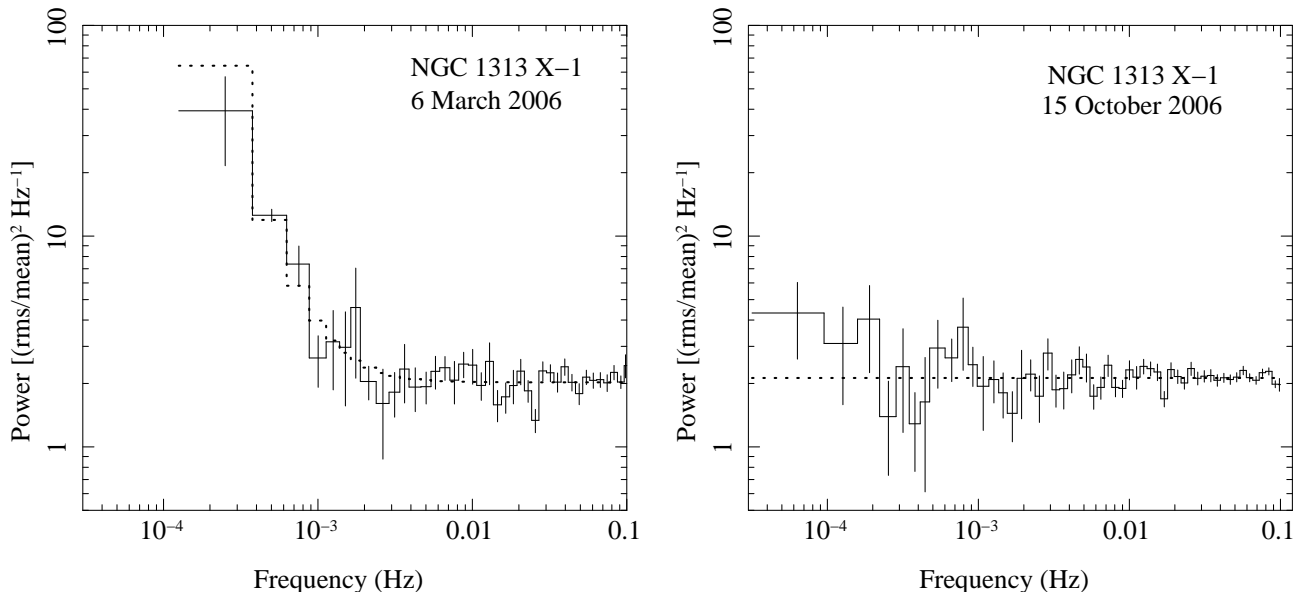
of about ~ 2 , and (ii) the emission was remarkably steady throughout the ~ 120 ks exposure. The soft and hard band emission and the hardness ratio also remained steady, implying that the spectrum of the ULX did not change substantially (see Fig. 1, *right panel*). Henceforth, throughout this work we refer to the 6 March observation as the high state and the 15 October one as the low state.

To quantify the variability, we have calculated the intrinsic source variability expressed in terms of the fractional variability amplitude ($F_{var} = (\sigma_{XS}^2 / \bar{x}^2)^{1/2}$, where σ_{XS}^2 is the variance after subtracting the contribution expected from measurement errors, and \bar{x} is the mean count rate (see Vaughan et al. 2003, and references therein). We used the background corrected lightcurves binned with 200 s to calculate F_{var} , listed in Table 1. While the measured F_{var} is consistent with no intrinsic variability during the low state, significant intrinsic variability is seen during the high state. We have also derived the power density spectra using the EPIC-pn lightcurves binned with 5 s. For the low state, we used the first ~ 79 ks continuous exposure in order to avoid the data gap and the flaring particle background seen towards the end of the observation (see Fig. 1). The light curves were divided into five equal segments and the PSDs of each segment was computed. The five individual PSDs were averaged and the errors were assigned to be the standard deviation at each frequency bin. The resultant PSDs (after binning) are shown in Figure 2. The PSD shows red-noise behavior at low frequencies for the hard state, while it is flat during the low one. A constant model fitted to the PSD for the low state resulted in a minimum $\chi^2 = 59.3$ for 52 degrees of freedom (dof). The best-fit constant power density is 2.12 ± 0.04 which is slightly higher than the power density of 2 expected from pure Poisson noise arising from photon counting statistics. The marginal higher

Table 1. Variability properties of NGC 1313 X-1

Energy band	6 March 2006			15 October 2006		
	Source (counts s ⁻¹)	Background (counts s ⁻¹)	$F_{var}(\%)^1$	Source (counts s ⁻¹)	Background (counts s ⁻¹)	$F_{var}(\%)^1$
0.2 – 10 keV	1.47 ± 0.09	0.016 ± 0.004	14.6 ± 0.6	0.77 ± 0.07	0.026 ± 0.006	2.3 ^{+0.9} _{-1.9}
0.2 – 2 keV	1.06 ± 0.08	0.009 ± 0.003	11.0 ± 0.8	0.55 ± 0.06	0.010 ± 0.004	2.9 ^{+1.0} _{-1.7}
2 – 10 keV	0.41 ± 0.05	0.006 ± 0.003	23.7 ± 1.2	0.22 ± 0.04	0.013 ± 0.004	< 4.3

¹Calculated from background subtracted lightcurve with 200 s bins.

**Figure 2.** Power density spectra of NGC 1313 X-1 derived from the EPIC-pn lightcurves obtained on 6 March 2006 and 15 October 2006

power density could arise from slight variation in the background level (see Fig. 1 *right panel*). Thus, we measure no significant intrinsic variability, consistent with the measured F_{var} (see Table 1). As expected, a constant power density model fit to the PSD of the high state resulted in a statistically unacceptable fit ($\chi^2/dof = 211.5/38$). Addition of a power-law component ($\propto \nu^{-\alpha}$) improved the fit significantly ($\chi^2/dof = 47.7/36$) with $\alpha = -2.25 \pm 0.30$. Interestingly a broken power-law model further improved the fit marginally ($\chi^2/dof = 40.9/34$). However, the parameters of the model are not well constrained and hence we conclude that the data is suggestive of a break, but no concrete inference can be made.

2.2 Spectral Analysis

We extracted EPIC-pn and MOS spectra from the two observations using circular regions with radii of 40'' centered at the position of NGC 1313 X-1. We also extracted background spectra using appropriate nearby circular regions free of sources. We created spectral response files using the SAS tasks `rmfgen` and `arfgen`. Spectral bins were chosen such that there was a minimum of 20 counts per spectral channel for the pn and the MOS data of March 2006 (high state). The high signal-to-noise EPIC-pn, MOS1 and MOS2 data extracted from the deep observation of Octo-

ber 2006 (low state) were grouped to minimum counts of 200, 50 and 50, respectively. These spectra were analyzed with `ISIS 1.4.9`. All spectra were fitted in the energy range 0.3 – 10 keV and the errors on the best-fit spectral parameters are quoted at a 90% confidence level.

We begin with the spectral analysis of the low state. A simple absorbed power law (PL) model was fitted individually to the pn and MOS spectra. Examination of the individual fits showed the photon indices and absorption columns obtained for three data sets were similar within errors and the fits had similar residuals. Therefore, we fitted the pn and MOS data jointly and used an overall normalization constant to account for possible differences in source extraction areas or calibration uncertainties. The simple power-law model resulted in a statistically unacceptable fit ($\chi^2/dof = 1484.0/674$). The ratio of the pn+MOS data and the power-law model is shown in Fig. 3 (*bottom panel*). This plot clearly shows a broad hump or a cutoff near 6 keV and a soft X-ray hump or excess emission in the 0.6 – 1.2 keV band. Similar spectra have been reported earlier for several ULXs (Feng & Kaaret 2005; Stobbart et al. 2006; Dewangan et al. 2006). Addition of a multicolor disk blackbody (MCD) component to the PL model improved the fit significantly ($\chi^2/dof = 807/672$). Replacing the PL with a cutoff PL further improved the fit ($\chi^2/dof = 717.3/671$). This kind of a high energy cut-

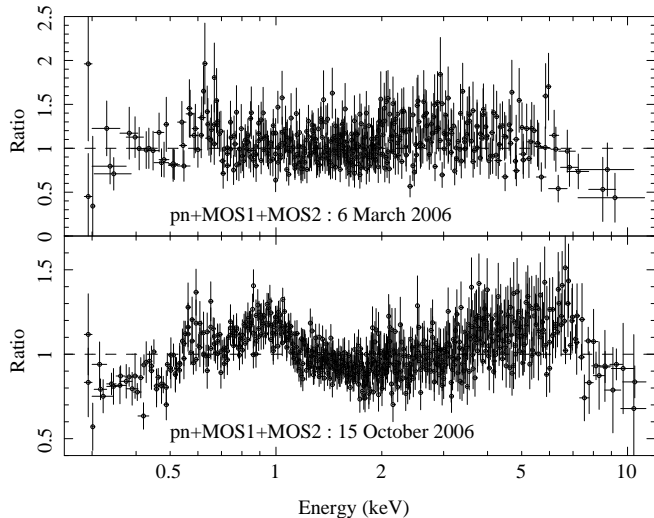


Figure 3. Ratios of observed pn+MOS data obtained on 6 March 2006 (*top panel*) and 15 October 2006 (*bottom panel*) and the best-fitting absorbed power-law models.

off is common among bright ULXs and is well described by thermal Comptonization in a relatively cool and optically thick plasma. (Agrawal & Misra 2006; Stobbart et al. 2006; Goad et al. 2006; Dewangan et al. 2006; Roberts 2007). To test such a scenario, we replaced the cutoff PL model with the thermal Comptonization model (nthcomp) described by Zdziarski et al. (1996) and Życki et al. (1999). The free parameters of the nthcomp model are the asymptotic power-law index ($\Gamma_{nthcomp}$), electron temperature (kT_e) and the seed photon temperature (kT_s). The electron scattering optical depth (τ) can be calculated from the asymptotic power-law photon index (Γ_{compth}) and electron temperature (kT_e) as follows

$$\alpha = \left[\frac{9}{4} + \frac{1}{(kT_e/m_e c^2)\tau(1 + \tau/3)} \right]^{1/2} - \frac{3}{2} \quad (1)$$

with $\Gamma_{nthcomp} = \alpha + 1$ (Sunyaev & Titarchuk 1980). Since a soft X-ray excess emission, described by an MCD, is clearly detected, it is simplistic to assume that this component provides the seed photons for the Comptonization. Therefore, the temperature of the soft excess and the seed photons were kept the same and varied together. The shape of the soft component was assumed to be that of a MCD. The MCD+nthcomp model provided a good fit ($\chi^2/dof = 717.9/671$) and the best-fit parameters are reported in Table (2). To confirm that the results do not depend on the Comptonization model used, we have fitted the data using the XSPEC model compTT (Titarchuk 1994; Hua & Titarchuk 1995; Titarchuk & Lyubarskij 1995) instead of nthcomp and obtained a $\chi^2/dof = 716.3/671$ with similar parameter values. In Fig. 4, we show the unfolded EPIC-pn spectrum, the best-fitting absorbed MCD+ncomp model in panel (a) (*upper curve*), and the deviations of the data from the model in panel (c). For clarity we show only the EPIC-pn data. Unlike XPSEC, the unfolded spectrum in ISIS is derived in a model-independent way as follows:

$$f_{unfold}(I) = \frac{[C(I) - B(I)]/\Delta t}{\int R(I, E)A(E)dE}, \quad (2)$$

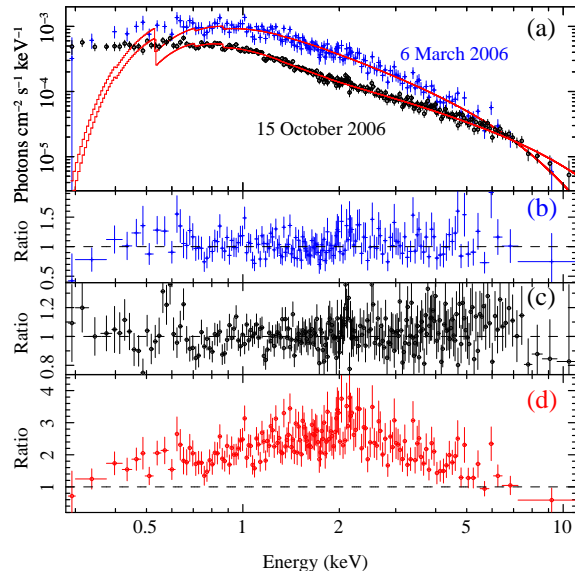


Figure 4. Results of spectral fitting to the EPIC-pn data obtained on high (6 March 2006) and low (15 October 2006) states. (a) *Lower plot*: Observed data for the high state and the best-fit model - thermal Comptonization in a cool, optically thick medium Unfolded (nthcomp); *Upper plot*: Observed data for the low state and the best-fit model MCD+nthcomp. (b) Deviations of the observed data of the high state from the best-fit absorbed nthcomp model. (c) Deviations of the observed data for the low state from the best-fit absorbed MCD+nthcomp model. (d) Difference in the shape of the spectra for the high and low states. The plot shows the deviations of the data of the low state from the best-fit model to the high state data but renormalized to match the fluxes.

where $C(I)$ is the number of total counts in the energy bin I , $B(I)$ is the number of background counts, Δt is exposure time, $R(I, E)$ is the normalized response matrix and $A(E)$ is the effective area at energy E . This definition produces a spectrum that is independent of the fitted model. The best-fit model has been over-plotted at the internal resolution of the ancillary response function. The spectrum and the model are expected to match only in the particular case of unit response matrix (Nowak 2005). Hence there is deviation between the model and the data points at low energies. Note that the *model independent* unfolded data points clearly shows a curvature at high energies, which signifies that the curvature is real and not a modeling artifact.

We then proceed to the spectral analysis of the pn and MOS data of the high state. As mentioned earlier in section 2, the extension of the ULX in the EPIC-pn image overlaps with the chip gap, hence a good fraction of the events at high energies were discarded as these events have poorly determined patterns. Consequently, the EPIC-pn and the MOS data have comparable signal-to-noise. Simple absorbed power-law model fitted separately to the pn, MOS1 and MOS2 data resulted in similar photon indices and we did not find significant differences in the residuals, therefore we present results based on joint spectral fitting of the pn and MOS data as before. The simple power law model resulted in a minimum $\chi^2 = 455.3$ for 440 dof. With a reduced $\chi^2 = 1.03$, a simple power-law model seems adequate and does not seem to warrant exploration of more

Table 2. Best-fit spectral model parameters for NGC 1313 X-1.

Parameters	6 March 2006 nthComp	15 October 2006 MCD+nThComp
$N_H(10^{21} \text{ cm}^{-2})$	2.50(fixed)	$2.50^{+0.16}_{-0.15}$
$kT_{in}(\text{ eV})^a$	–	227
f_{MCD}^b	–	$1.24^{+0.15}_{-0.12} \times 10^{-12}$
$kT_S(\text{ eV})^c$	122 ± 15	227^{+14}_{-12}
$kT_e(\text{ keV})^d$	$1.67^{+0.28}_{-0.19}$	$2.27^{+0.18}_{-0.15}$
Γ^e	$2.02^{+0.05}_{-0.04}$	1.67 ± 0.03
f_{comp}^f	$7.51^{+0.24}_{-0.23} \times 10^{-12}$	$(3.1 \pm 0.1) \times 10^{-12}$
f_X^g	$7.51^{+0.24}_{-0.23} \times 10^{-12}$	$4.34^{+0.21}_{-0.18} \times 10^{-12}$
L_{bol}^h	17.9×10^{39}	11.9×10^{39}
χ^2_{min}/dof	421.4/439	717.9/671

^aInner disk temperature of disk blackbody model which is tied to kT_S .

^b0.3 – 10 keV flux of the MCD component in $\text{ergs cm}^{-2} \text{ s}^{-1}$.

^cTemperature of the seed photon source of the Comptonization model

^dHot electron plasma temperature.

^ePhoton Index of the Comptonization model.

^f0.3–10 keV flux of the Comptonization model in $\text{ergs cm}^{-2} \text{ s}^{-1}$.

^gUnabsorbed 0.3 – 10 keV flux in $\text{ergs cm}^{-2} \text{ s}^{-1}$.

^hUnabsorbed bolometric luminosity in ergs s^{-1} .

complex models. Indeed Feng & Kaaret (2006) were able to model several similar quality data of this source with a simple power-law. However, the analysis of better quality data described above suggests that the spectrum of the source could be more complex. Moreover, as we show below, there is evidence for a more complex spectral shape even for this statistically poorer data set. We have plotted the ratio of the pn+MOS1+MOS2 data and the best-fit PL model in Figure 3(*upper panel*). The absorbed power-law model is a good description of the data below ~ 6 keV. There is a likely cut-off or curvature at high energies. To verify the possible high energy turnover of the X-ray spectra, we replaced the PL component by a cut-off PL. The absorbed cut-off PL model yielded $\Delta\chi^2 = -19.9$ for one additional parameter as compared to the absorbed PL model. This is an improvement at a significance level of $> 99.99\%$ based on the Maximum Likelihood Ratio test. The absorbed nthcomp model provided a similar fit with $\chi^2/dof = 421.4/439$. In Figure 4, we show the unfolded EPIC-pn spectrum, the best-fitting absorbed nthcomp model in panel (a) marked as 6 March 2006 and the deviations in panel (b). Note that, similar to the low state data set, the *model independent* unfolded data points clearly show a curvature at high energies which again signifies that the curvature is real and not a modeling artifact. It is also clear from the model independent unfolded data that both the flux and spectral shape varied between the two data sets. This is highlighted in panel (d) of the Figure which shows the deviations of the low state data from the renormalized best fit model of the high state. We have also investigated

the possible presence of a disk component similar to that observed in the low state. Addition of an MCD component to the nthcomp model with MCD kT_{in} tied to the nthcomp kT_S did not improve the fit. We calculated an upper-limit of $L_{MCD} < 1.4 \times 10^{39} \text{ ergs s}^{-1}$ for the bolometric luminosity of the MCD component in the 0.001 – 100 keV band. We also fixed the MCD kT_{in} at the value obtained for the low state and calculated the upper limit, $L_{MCD} < 6.3 \times 10^{39} \text{ ergs s}^{-1}$.

3 ACCRETION DISK GEOMETRY

As revealed in Table 2, the low state spectrum of the source can be described with a thermal Comptonization and a disk black body model. The luminosity of the disk black body (i.e. the MCD model) is $L_{MCD} \sim 4 \times 10^{39} \text{ ergs/s}$, while that of the thermal Comptonization is $\sim 7.7 \times 10^{39} \text{ ergs/s}$. Using the XSPEC model function for the model “nthcomp”, one can estimate the amplification factor, $A \equiv L_c/L_s \sim 4.8$, where L_c and L_s are the luminosities of the Comptonization component and the seed photon input. This allows an estimate of $L_s \sim 1.6 \times 10^{39} \text{ ergs/s}$. This is consistent with an accretion disk geometry where a standard cold accretion disk is terminated at radius R_{tr} and the inner region is an hot plasma. The inner hot plasma Comptonizes photons from the outer disk producing high energy photons. For consistency, the seed photon spectral shape for the Comptonization model is taken to be a disk black body emission at the same temperature as the disk emission observed. In this model, the fraction of the cold disk photons that enter the inner hot region is related to the solid angle which the hot region makes with the outer disk. The observed fraction of the luminosity of the seed photon component as compared to the disk luminosity, $L_S/L_{MCD} \sim 0.4$ suggests a solid angle of $\Delta\Omega \sim 0.4 \times 2\pi \sim 0.8\pi$. Note that $L_S/L_{MCD} \lesssim 1$ is a consistency check for the geometry proposed. In this geometry, it would be difficult to reconcile $L_S > L_{MCD}$ and $L_S \ll L_{MCD}$ would require an unphysical small subtending solid angle.

The normalization of the disk component provides an estimate of the transition radius

$$R_{tr} \sim 10^9 \text{ cm} \left(\frac{\kappa}{1.7} \right)^2 \left(\frac{\cos i}{0.5} \right)^{-1/2} \quad (3)$$

where i is the inclination angle and κ is the color factor. In the standard accretion disk theory (Shakura & Sunyaev 1973), the luminosity of a truncated disk is given by

$$L_{MCD} \sim \frac{3GM\dot{M}}{2R_{tr}} \quad (4)$$

where M is the mass of the black hole and \dot{M} is the accretion rate. The total bolometric luminosity, $L_T = (L_C - L_S) + L_{MCD}$ can be expressed as $L_T = \eta\dot{M}c^2$ where η is the efficiency of the system. Thus, the mass of the black hole can be estimated to be

$$\begin{aligned} M &\sim \frac{2c^2}{3G} \eta R_{tr} \frac{L_{MCD}}{L_T} \\ &\sim 200 M_\odot \left(\frac{\eta}{0.1} \right) \left(\frac{R_{tr}}{10^9 \text{ cm}} \right) \left(\frac{L_{MCD}/L_T}{0.43} \right) \end{aligned} \quad (5)$$

The Eddington luminosity for a $200M_\odot$ solar mass black hole is $L_{Edd} = 2.5 \times 10^{40} \text{ ergs/s}$ and hence the source is

radiating at an Eddington ratio of $L_T/L_{Edd} \sim 0.37$. The Schwarzschild radius turns out to be $r_s \equiv 2GM/c^2 \sim 6 \times 10^7$ cm, making the transition radius $R_{tr} \sim 17r_s$.

Thus the spectral shape of the low state is totally consistent with a scenario where a $\sim 200M_\odot$ solar mass black hole is surrounded by a standard accretion disk which is truncated at $\sim 17r_s$. The disk produces a multi temperature emission which is observed as a soft component. The inner hot region is geometrically thick and subtends a solid of angle of $\sim 0.8\pi$ to the disk outside. This allows it to Comptonize photons from the outer disk producing the main Comptonized component. The system is radiating at a Eddington ratio ~ 0.4 with a standard radiation efficiency $\eta \sim 0.1$.

The spectrum of the high state can be adequately fitted with a single thermal Comptonization model. The luminosity of the model is $\sim 16.6 \times 10^{39}$ ergs/s and an Amplification factor, $A \sim 2.5$. The input seed photon luminosity turns out to be $\sim 6.5 \times 10^{40}$ ergs/s. This is significantly higher by a factor of ~ 4 of the seed photon luminosity for the low state. If, like in the low state, the seed photons are due to an external truncated accretion disk, the direct emission from such a disk is expected to be $L_{MCD} \sim \frac{L_s}{0.4} \sim 1.6 \times 10^{41}$ ergs s^{-1} which would have been easily detected. The upper-limit to the observed disk emission, however, is only 6.3×10^{39} ergs s^{-1} . Thus the absence of a soft component in the spectrum argues against such a geometry. Moreover, if the input seed photon shape is taken as disk black body emission, the inner disk temperature turns out to be 0.2 keV which is similar to that of the low state, despite the factor of four change in luminosity. The luminosity of a truncated accretion disk is $\propto \dot{M}/R_{tr}$ while the temperature is $\propto \dot{M}^{1/4}/R_{tr}^{3/4}$. Thus a near constant temperature accompanied by a factor of four increase in luminosity would imply that the accretion rate \dot{M} has increased by a factor of ~ 8 while the truncation radius has increased by a factor of ~ 2 . The large factor of ~ 8 change in the accretion rate is not reflected in the change in the total luminosity of the source, which is only a factor of ~ 1.5 higher than the low state. Thus a truncated accretion disk with an inner hot region does not seem to be a viable model for the high state of the source.

An alternate geometry for the high state spectrum is that of a corona covering an optically thick and geometrically thin disk (Haardt & Maraschi 1993; Liang & Price 1977). In this sandwich model, a fraction of the total gravitational power is dissipated in the disk, P_d and the rest in the corona P_c . The disk photons get Comptonized by the overlying corona and hence only a thermal Comptonized spectrum is observed. A fraction $\xi \lesssim 0.5$ of the Comptonized photons impinge back on to the underlying disk and are absorbed. The luminosity of the seed photon is then $L_s = P_d + \xi L_c$, where L_c is the luminosity of the Comptonized photon. The observed total luminosity $L_o = L_c(1-\xi) = P_d + P_c$. Defining the Compton amplification factor $A \equiv L_c/L_s$, the dissipated powers can be related to the total luminosity as,

$$P_c = \frac{A-1}{(1-\xi)A} L_o \quad (6)$$

and

$$P_d = \frac{1-\xi A}{(1-\xi)A} L_o \quad (7)$$

The geometry is valid only for $\xi < \xi_{max} = 1/A$. In the absence of feedback, $\xi = 0$, $P_d = L_o/A = L_d$ and $P_c = L_o - P_d$. In the other extreme of maximal feedback $\xi = \xi_{max}$, $P_d = 0$ and $P_c = L_o$.

For the high state, the spectrum can be interpreted in terms of the corona model, with the seed photon luminosity assumed to be a black body. The seed photon temperature turns out to ~ 0.12 keV and an amplification factor of $A \sim 2.54$ which imposes an upper limit on $\xi_{max} \sim 0.4$. Thus with a $\xi \lesssim 0.5$ and absence of any other strong soft component, the spectrum is consistent with the corona model. The size of the corona region R_c can be estimated using $\sigma T_s^4 2\pi R_c^2 = L_s = L_o/(1-\xi)A$. For $L_o \sim 1.7e40$ ergs/sec, $\xi \sim 0.25$ and $A \sim 2.5$, $R_c \sim 3 \times 10^9$ cm. For a $200M_\odot$ solar mass black hole this corresponds to $\sim 50r_s$. If there is an standard accretion disk beyond this radius, its temperature would be < 0.1 keV and would have a luminosity $< 2 \times 10^{39}$ ergs/s. Such a emission would not have been detected. The Eddington ratio for this state turns out be ~ 0.7 as compared to ~ 0.4 for the low one.

The temporal variability of the high state spectrum allows us to further constrain and verify the corona geometry. The fractional root mean squared (rms) variability as a function of energy is shown in Figure (5). The simplest interpretation would be that the observed variability is induced by variations in the coronal power P_c . From equations (6) and (7), the amplification can be written as

$$A(T_e, T_s, \tau) = \frac{P_d + P_c}{P_d + \xi P_c} \quad (8)$$

and the seed photon luminosity as

$$L_s = \frac{P_d + \xi P_c}{1-\xi} \propto T_s^4 \quad (9)$$

A variability in $P_c(t) = P_{c0}(1 + \delta P_c(t))$, will induce corresponding variation in the amplification, δA and the seed photon temperature δT_s . Assuming that the optical depth τ of the corona does not vary, the above two equations determine the time variability of $T_e(t)$ and $T_s(t)$ as a function of $\delta P_c(t)$. The time dependent spectrum can then be obtained from $T_e(t)$ and $T_s(t)$. The standard deviation of the time dependent spectrum at different energy bands then provides a predicted rms variation that can be compared with the observed values. For $\xi = 0.25$, (solid line in Figure 5), the predicted curve is consistent with the observations. For comparison, curves for $\xi = 0$ (dashed line) and $\xi = \xi_{max} = 0.39$ (long dashed line) are also plotted in the figure. Note that apart from the overall normalization, the predicted rms versus energy plot depends only on ξ , since the rest of the parameters are determined by the time-averaged spectral fitting. Thus the coronal geometry naturally explains the energy dependent variability of the source.

As the coronal power increases, the electron temperature should also increase making the spectrum harder. Thus the model predicts a correlation between flux and hardness ratio which is indeed seen in the variability. In the left panel of Figure (1) the hardness ratio is observed to increase with flux. While the qualitative behavior is consistent, a quantitative evaluation is unfortunately not possible. Such a quantitative estimate would require a fairly accurate knowledge of the response of the instrument to convert the model photons into counts. As mentioned earlier, for this observation, the

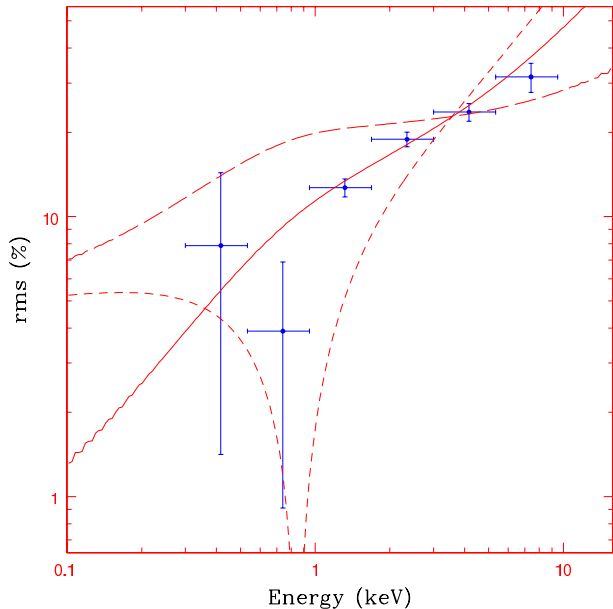


Figure 5. The observed rms variation with energy for the low state data. The predicted rms variation for $\xi = 0.25$ (solid line), $\xi = 0$ (dashed line) and for $\xi = \xi_{max} = 0.33$ (long dashed line)

source extension overlaps with the EPIC-pn chip gap and a large fraction of events have uncertain pattern. These events with poor spectral calibration although excluded from the spectral analysis were included in the temporal analysis. Excluding them from the temporal analysis renders the statistics too poor but their inclusion means that their energies are not well constrained.

The spectrum and rms variability of the source in the high state is totally consistent with a geometry where a corona covers an underlying disk in a sandwich model. The photons emitted from the disk are Comptonized by the corona and only a single thermal component is seen. A fraction $\xi \sim 0.25$ of the Comptonized photons impinge back on the disk and are absorbed. The size of the coronal region is $\sim 50r_s$ for a $200M_\odot$ black hole and the Eddington ratio is ~ 0.7 .

4 SUMMARY AND DISCUSSION

We have investigated the spectral and temporal behavior of the bright ULX NGC 1313 X-1 using two long *XMM-Newton* observations. On 6 March 2006, the ULX was in a high flux state with an average count rate of ~ 1.5 counts/s, while on in October 2006 the count rate had decreased to ~ 0.78 counts/s. The main results of the analysis are as follows.

The spectrum of the low state shows definite evidence for a high energy curvature. It can be fitted with a thermal Comptonization model with an optical depth $\tau \sim 15$ and temperature $kT_e \sim 2.3$ keV. An additional soft component, which can be modeled as a disk black body emission with a inner disk temperature of $kT_{in} \sim 0.23$ keV, is required for the spectral fit. The flux from the source is steady with an upper limit on the rms variability of $< 3\%$.

The spectral shape during the high state is distinctively

different from that of the low state. The entire spectrum can be fitted by a single thermal Comptonization model with an optical depth $\tau \sim 13.5$ and temperature $kT_e \sim 1.67$ keV. There is no evidence for any additional soft component. The source is highly variable in this state with an rms variability of 14%. The associated temporal and spectral difference between the two observations indicates that the source underwent a true state transition.

For a standard radiative efficiency of ~ 0.1 , the spectrum of the low state is completely consistent with a model where a $\sim 200M_\odot$ black hole is surrounded by a standard accretion disk truncated at a radius of $\sim 17r_s$ ($r_s \equiv 2GM/c^2$). This outer disk gives rise to the soft component. There is an inner hot region which subtends a solid angle of $\sim 0.8\pi$ to the outer disk. Hence photons from the outer disk enter the inner hot region, get Comptonized, and are observed as the primary thermal Comptonized component. The system has an Eddington ratio of $L_T/L_{Edd} \sim 0.4$.

The spectrum of the high state is not compatible with a truncated disk and inner hot region geometry. This is primarily inferred by the absence of any strong soft component, despite a four fold increase in the input soft photon flux at nearly the same temperature. The difference in disk geometry further confirms that a true state transition has occurred between the two observations.

The spectrum as well as the *rms variability as a function of energy* of the high state, is completely consistent with a model where a geometrically thin disk has a hot corona overlying it. Photons from the underlying disk get Comptonized in the corona and a single thermal Comptonization model is observed. A fraction ~ 0.25 of the Comptonized photons impinge back on the disk and are absorbed. The observed variability can be naturally ascribed to variations in the coronal power. The size of the coronal region is $\sim 50r_s$ and the Eddington ratio during this state is ~ 0.7 .

The low state of NGC 1313 X-1 seems to be analogous to the low hard state of Galactic X-ray binaries, which can also be broadly explained in terms of a truncated accretion disk and an hot inner region. Similarly the coronal geometry for the high state is the same as the one invoked for the high soft state of Galactic X-ray binaries. However, this is an important difference between the hot region/corona of Galactic sources and NGC 1313 X-1. The hot region/corona of Galactic sources is optically thin ($\tau \sim 1$) and has a high temperature, ~ 50 keV. The hot region/corona for NGC 1313 X-1, is optically thick ($\tau \gtrsim 10$) and has a much lower temperature ~ 2 keV. This difference is more than just quantitative. Optically thin plasmas with electron temperatures ~ 50 keV can be in a two-temperature state, with the proton temperature being much higher (a factor of ~ 1000) than that of the electron gas (Shapiro et al. 1976). Such plasmas are gas pressure dominated. Optically thick and low temperature plasmas cannot have such a two-temperature structure and would be radiation pressure dominated. Thus, such plasmas would have to be dynamically different from those observed in Galactic sources.

With an Eddington ratio of ~ 0.5 , the only difference between NGC 1313 X-1 and Galactic black hole systems seems to be the larger mass of the black hole. However, the X-ray spectra of bright AGN reveal the presence of an optically thin and hot plasma similar to those inferred for

Galactic sources. It is not clear why AGN with a $\sim 10^{6-9} M_{\odot}$ black hole mass have similar hot region/corona as $\sim 10 M_{\odot}$ Galactic black holes, but ULX with intermediate masses have qualitatively different plasmas. The broadband X-ray spectra of BHBs in their strongly Comptonized, very high state (VHS) require thermal Comptonization in an optically thick ($\tau \sim 2 - 3$) and relatively cool ($kT_e \sim 10$ keV) plasma in addition to multi-color disk blackbody emission from a truncated disk and a power-law extending to high energies (Done & Kubota 2006). The curvature produced by the low temperature thermal Comptonization component in BHBs could be similar to the ~ 5 keV curvature seen in the ULX spectra. Furthermore, many narrow-line Seyfert 1 galaxies and quasars with high Eddington ratio show soft X-ray excess emission with $kT \sim 200$ eV above a hard power-law. The soft excess emission can be modeled with Thermal Comptonization in an optically thick and cool plasma (see e.g., Dewangan et al. 2007; Middleton et al. 2008). Perhaps the ~ 5 keV curvature observed in ULX, the ~ 0.2 keV soft X-ray excess seen in many AGN, and the ~ 10 keV thermal Comptonization seen in strongly Comptonized VHS of BHB are all physically the same continuum components. There may be an additional hard X-ray (> 10 keV) power-law in ULX which would then be analogous to the X-ray power-law seen in AGN at $\gtrsim 2$ keV and in VHS of BHBs seen at $\gtrsim 10$ keV. However, at this stage such a conjecture would be speculative.

An alternate to the interpretation presented here is that the source harbors a $\sim 5 M_{\odot}$ black hole with super Eddington accretion (Shakura & Sunyaev 1973; King 2008). For such high accretion rates, the luminosity does not scale with \dot{M} , and instead is given by $L \sim L_{Edd}(1 + \log(\dot{M}/\dot{M}_E))$. Moreover, the characteristic radius at which the luminosity is released is $\sim (27/4)(\dot{M}/\dot{M}_E)r_s$, which is much larger than the standard value of $\sim 5r_s$. The luminosity is also expected to be further enhanced by some moderate beaming. Such an interpretation is attractive because (a) it does not require exotic formation and accretion mechanism needed to explain intermediate mass black holes, (b) the high accretion rates required are perhaps expected when there is thermal time scale mass transfer from donor stars and (c) it explains naturally why the spectra of ULX are distinct from Galactic sources and AGN which are sub-Eddington sources. However, the absence of a simple representation of the expected model spectrum does not allow for detailed spectral analysis. King (2009) associate the soft excess seen in some ULX as emission from such a super Eddington disk. This is reasonable if the soft excess is the energetically dominant component and not for cases like the low state of NGC 1313 X-1, where the soft component is less luminous than the main Comptonization one. Another issue is the factor of ~ 2 luminosity variability between the low and high state of NGC 1313 X-1. Since luminosity varies as $\log(\dot{M}/\dot{M}_E)$ this would imply a large accretion rate variation which in turn would imply a large variation in the characteristic radius $\propto \dot{M}$. Such a large variation in radius would result in a significant change in the characteristic temperature of the disk, which is not observed. King (2009) invoke variations in the moderate beaming factor to explain such observed variations, which although plausible is rather ad hoc. Finally, if the super Eddington accretion model is correct, then the self consistent standard disk modeling which explains both

the spectra as well as the variability versus energy, has to be considered as a coincidence. What is required is a better theoretical prediction of the super Eddington disk spectra which may have to include the possibility of a additional dominant Comptonization component.

In the standard disk framework, there is also a need for better theoretical understanding of a radiation pressure dominated corona as well as a hot inner region. The dynamics of such structures needs to be studied and ascertained that they are viable stable systems. Perhaps more importantly, the results presented in this work need to be confirmed by longer observations of the same source as well as other sources which show similar characteristics. The latter is important since there may be different kinds of ULX, even among the brightest ones.

ACKNOWLEDGMENTS

This work is based on observations obtained with *XMM-Newton*, an ESA science mission with instruments and contributions directly funded by ESA Member States and the USA (NASA). This research has made use of data obtained through the High Energy Astrophysics Science Archive Research Center Online Service, provided by the NASA/Goddard Space Flight Center. The long 123 ks observation was supported by the NASA grant NNX07AE99G.

REFERENCES

- Agrawal V. K., Misra R., 2006, ApJL, 638, L83
- Begelman M. C., 2002, ApJL, 568, L97
- Colbert E. J. M., Miller M. C., 2005, in Novello M., Perez Bergliaffa S., Ruffini R., eds, The Tenth Marcel Grossmann Meeting. On recent developments in theoretical and experimental general relativity, gravitation and relativistic field theories Observational Evidence for Intermediate-Mass Black Holes in Ultra-Luminous X-Ray Sources. pp 530–+
- Devi A. S., Misra R., Agrawal V. K., Singh K. Y., 2007, ApJ, 664, 458
- Dewangan G. C., Griffiths R. E., Dasgupta S., Rao A. R., 2007, ApJ, 671, 1284
- Dewangan G. C., Griffiths R. E., Rao A. R., 2006, ApJL, 641, L125
- Dewangan G. C., Miyaji T., Griffiths R. E., Lehmann I., 2004, ApJL, 608, L57
- Dewangan G. C., Titarchuk L., Griffiths R. E., 2006, ApJL, 637, L21
- Done C., Kubota A., 2006, MNRAS, 371, 1216
- Feng H., Kaaret P., 2005, ApJ, 633, 1052
- Feng H., Kaaret P., 2006, ApJL, 650, L75
- Feng H., Kaaret P., 2007, ApJL, 660, L113
- Goad M. R., Roberts T. P., Reeves J. N., Uttley P., 2006, MNRAS, 365, 191
- Haardt F., Maraschi L., 1993, ApJ, 413, 507
- Hua X.-M., Titarchuk L., 1995, ApJ, 449, 188
- Kaaret P., Corbel S., Prestwich A. H., Zezas A., 2003, Science, 299, 365
- Kaaret P., Feng H., 2007, ApJ, 669, 106
- Kaaret P., Simet M. G., Lang C. C., 2006, ApJ, 646, 174

- King A. R., 2008, MNRAS, 385, L113
King A. R., 2009, MNRAS, 393, L41
King A. R., Davies M. B., Ward M. J., Fabbiano G., Elvis M., 2001, ApJL, 552, L109
Kubota A., Mizuno T., Makishima K., Fukazawa Y., Kotoku J., Ohnishi T., Tashiro M., 2001, ApJL, 547, L119
La Parola V., Peres G., Fabbiano G., Kim D. W., Bocchino F., 2001, ApJ, 556, 47
Liang E. P. T., Price R. H., 1977, ApJ, 218, 247
Méndez B., Davis M., Moustakas J., Newman J., Madore B. F., Freedman W. L., 2002, AJ, 124, 213
Middleton M., Done C., Ward M., Gierlinski M., Schurch N., 2008, ArXiv e-prints
Miller J. M., Fabbiano G., Miller M. C., Fabian A. C., 2003, ApJL, 585, L37
Miller J. M., Fabian A. C., Miller M. C., 2004, ApJ, 607, 931
Mirabel I. F., Rodríguez L. F., 1999, ARA&A, 37, 409
Mucciarelli P., Casella P., Belloni T., Zampieri L., Ranalli P., 2006, MNRAS, 365, 1123
Nowak M., 2005, Ap&SS, 300, 159
Roberts T. P., 2007, Ap&SS, 311, 203
Shakura N. I., Sunyaev R. A., 1973, A&A, 24, 337
Shapiro S. L., Lightman A. P., Eardley D. M., 1976, ApJ, 204, 187
Stobbart A.-M., Roberts T. P., Wilms J., 2006, MNRAS, 368, 397
Strohmayer T. E., Mushotzky R. F., 2003, ApJL, 586, L61
Strohmayer T. E., Mushotzky R. F., Winter L., Soria R., Uttley P., Cropper M., 2007, ApJ, 660, 580
Sugihō M., Kotoku J., Makishima K., Kubota A., Mizuno T., Fukazawa Y., Tashiro M., 2001, ApJL, 561, L73
Sunyaev R. A., Titarchuk L. G., 1980, A&A, 86, 121
Titarchuk L., 1994, ApJ, 434, 570
Titarchuk L., Lyubarskij Y., 1995, ApJ, 450, 876
Vaughan S., Edelson R., Warwick R. S., Uttley P., 2003, MNRAS, 345, 1271
Winter L. M., Mushotzky R. F., Reynolds C. S., 2006, ApJ, 649, 730
Zdziarski A. A., Gierliński M., 2004, Progress of Theoretical Physics Supplement, 155, 99
Zdziarski A. A., Johnson W. N., Magdziarz P., 1996, MNRAS, 283, 193
Życki P. T., Done C., Smith D. A., 1999, MNRAS, 309, 561